metals

MDPI

Article

Electrochemical Corrosion Behavior of HiPIMS-Deposited Diamond-like Carbon (DLC) Coatings on AISI 52100 Steel in Synthetic Seawater

Ilse Arreola [1], Engelbert Huape [2], Martin Flores [3], Héctor Carreón [1], José Bernal [4] and Ariosto Medina [1,*]

[1] Institute of Research in Metallurgy and Materials, Universidad Michoacana de San Nicolás de Hidalgo, Morelia 58030, Mexico; 2459341b@umich.mx (I.A.); hcarreon@umich.mx (H.C.)
[2] Faculty of Mechanical Engineering, Universidad Michoacana de San Nicolás de Hidalgo, Morelia 58030, Mexico; engelbert.huape@umich.mx
[3] Department of Project Engineering, Centro Universitario de Ciencias Exactas e Ingenierias (CUCEI), University of Guadalajara, Zapopan 45129, Mexico; martin.fmartinez@academicos.udg.mx
[4] National Technological Institute of Mexico, Technological Institute of Orizaba, Orizaba 94320, Mexico; jberponce@gmail.com
* Correspondence: ariosto.medina@umich.mx

Abstract

This manuscript evaluates the electrochemical corrosion resistance of diamond-like carbon (DLC) coatings deposited via High-Power Impulse Magnetron Sputtering (HiPIMS) on AISI 52100 steel in synthetic seawater. While AISI 52100 steel is valued for its hardness, it is highly susceptible to localized and uniform corrosion in chloride-rich marine environments. In this study, samples were characterized using Raman spectroscopy to analyze sp^2/sp^3 bonding, and their corrosion behavior was assessed through potentiodynamic polarization, linear polarization resistance (LPR), and electrochemical impedance spectroscopy (EIS) over 24 h of immersion. Results demonstrated that the DLC coatings significantly enhanced electrochemical stability, shifting corrosion potentials toward more noble values and reducing the corrosion current density from $(1.81 \pm 0.12) \times 10^{-7}$ to $(1.03 \pm 0.09) \times 10^{-9}$ mA·cm^{-2}. EIS data revealed high polarization resistance and effective barrier properties, despite a calculated total porosity of 3.06% resulting from intrinsic micro-defects. Although localized subsurface degradation and minor flaking were observed at defect sites, the HiPIMS-deposited DLC coatings effectively mitigated the corrosive impact of synthetic seawater, providing a significant contribution to the electrochemical barrier despite the persistence of electrolyte accessibility mediated by localized defects.

Keywords: DLC; HiPIMS; AISI 52100; EIS; porosity; Raman

Check for updates

Academic Editor: Renato Altobelli Antunes

Received: 27 April 2026
Revised: 30 May 2026
Accepted: 30 May 2026
Published: 4 June 2026

Copyright: © 2026 by the authors. Licensee MDPI, Basel, Switzerland. This article is an open access article distributed under the terms and conditions of the Creative Commons Attribution (CC BY) license.

1. Introduction

AISI 52100 steel (equivalent to 100Cr6) is a high-carbon, chromium bearing steel widely used in precision mechanical systems due to its exceptional hardness, resistance to rolling contact fatigue, and wear behavior under severe loading conditions [1–3]. These properties make it an attractive substrate for demanding tribological applications, including bearings, shafts, and contact components operating under cyclic mechanical stress. However, despite its favorable mechanical response, AISI 52100 exhibits significant susceptibility to electrochemical degradation in chloride-containing environments, where localized corrosion and widespread dissolution can compromise surface integrity and accelerate premature failure [2,3]. This limitation becomes particularly critical in marine

or humid service conditions, where corrosion-assisted degradation can act synergistically with wear processes.

Therefore, surface engineering strategies have become essential for extending the service life of AISI 52100 steel in aggressive environments. Among these, diamond-like carbon (DLC) coatings have emerged as a technologically relevant solution due to their combination of high hardness, low coefficient of friction, chemical inertness, and barrier properties against the diffusion of aggressive ionic species [4–8]. DLC coatings consist of metastable amorphous carbon structures containing varying proportions of tetrahedral (sp3) and trigonal (sp2) carbon bonds, where the relative configuration of the bonds strongly influences hardness, residual stress, tribological behavior, and electrochemical stability [4–8]. In corrosive environments, dense DLC coatings can substantially restricting the access of the electrolyte to the metallic substrate from the electrolyte, significantly reducing corrosion kinetics and delaying interfacial degradation [9–14].

Despite these advantages, the long-term corrosion behavior of DLC coatings is intrinsically dependent on coating density, the population of structural defects, the residual stress state, and adhesion to the substrate [4,6,7]. Defects such as pores, microcracks, or micro fissures can serve as preferential diffusion pathways for chloride ions, allowing localized electrochemical attack at the coating/substrate interface and ultimately leading to interfacial delamination [9–11,15]. Consequently, the electrochemical behavior of DLC systems cannot be interpreted solely in terms of the carbon layer itself, but rather as a coupled response involving the coating architecture, substrate properties, and interfacial stability.

Achieving durable adhesion of DLC coatings to high-hardness bearing steels such as AISI 52100 remains a significant technical challenge. This substrate exhibits high hardness, carbide heterogeneity, and a substantial difference in elastic modulus compared to amorphous carbon coatings conditions that promote interfacial stress concentration and increase the coating's susceptibility to failure under service conditions [1,4,6]. Conventional DC magnetron sputtering, although widely used for carbon film deposition, often produces coatings with limited plasma ionization, reduced adatom mobility, and decreased film densification, which can result in higher defect density and weaker interfacial bonding [16–18]. In the present study, the HiPIMS process was operated using pulse frequencies of 300 Hz and pulse amplitudes between 50 and 200 µs, promoting high instantaneous power densities and enhanced plasma ionization during deposition. These conditions are associated with increased ion bombardment and improved coating densification compared to conventional DC sputtering [16–19]. These characteristics make HiPIMS a particularly attractive deposition route for demanding substrates such as AISI 52100 steel.

Although numerous investigations have been conducted on the tribological behavior of DLC coatings, comparatively fewer studies have focused on the electrochemical corrosion response of DLC systems deposited by HiPIMS on high-carbon bearing steels under marine exposure conditions [11–13]. Furthermore, the interaction between substrate condition, coating integrity, electrochemical barrier performance, and defect-mediated degradation has not yet been fully elucidated. In particular, the effect of pre-heat treatment of AISI 52100 steel on subsequent corrosion behavior and coating response has received little attention.

Electrochemical characterization methods, such as potentiodynamic polarization, linear polarization resistance (LPR), and electrochemical impedance spectroscopy (EIS), provide valuable information on corrosion kinetics, barrier effectiveness, and interfacial degradation mechanisms in coated metal systems [15,20–23]. Similarly, Raman spectroscopy remains a powerful tool for evaluating the structural organization of DLC through D/G band analysis, enabling an indirect assessment of bonding characteristics associated with film stability [4,5,8]. Combined with post-corrosion microstructural observations, these

techniques allow for a comprehensive understanding of degradation mechanisms in carbon-based protective coatings. Chloride-containing marine environments are particularly aggressive for high-carbon steels because chloride ions destabilize corrosion-product layers, promote localized electrochemical activity, and accelerate interfacial degradation processes. In prolonged immersion conditions, corrosion-product accumulation may transiently modify the electrochemical response of steel surfaces without providing durable passivation, owing to the continued aggressive action of chloride-containing species [24–27].

Three conditions were evaluated: AISI 52100 steel in its original state (M1), heat-treated steel (M2), and steel coated with DLC deposited using a chromium-assisted HiPIMS architecture (M3). The objective of this study evaluates the electrochemical corrosion of Diamond-Like Carbon coatings (DLC) deposited by High-Power Impulse Magnetron Sputtering (HiPIMS). This research focuses specifically on the role of steel substrate and its subsequent impact on the coating's integrity when exposed to synthetic seawater.

2. Materials and Methods

AISI 52100 bearing steel specimens were used as substrate material under three experimental conditions: raw steel (M1), heat-treated steel (M2), and diamond-like carbon (DLC) coated steel (M3). Disc-shaped samples with dimensions of 25.4 mm in diameter and 5 mm in thickness were machined from the base material. For the heat-treated condition (M2), the samples were subjected to an austenitizing treatment at 864 °C for 20 min, followed by rapid cooling in oil, in order to modify the microstructural condition of the substrate and the mechanical response prior to electrochemical evaluation. No post-quench tempering treatment was applied prior to DLC deposition. Surface preparation was performed using a sequential grinding process with silicon carbide abrasive papers up to 2000 grit, followed by polishing with polycrystalline diamond suspensions of 6 μm, 3 μm, and 0.05 μm, achieving a suitable for coating deposition and electrochemical testing. Subsequently, the samples were ultrasonically cleaned in acetone and isopropyl alcohol for 15 min each and dried under a nitrogen flow.

DLC (M3) coatings were deposited using high-power pulsed magnetron sputtering (HiPIMS). Prior to deposition, the substrates were cleaned with argon plasma, followed by chromium-assisted ion bombardment pretreatment to activate the surface and enhance interfacial adhesion. A chromium-based intermediate layer was incorporated to optimize coating adhesion and reduce stress concentration at the substrate/coating interface. The deposition parameters used are summarized in Table 1. During the deposition process, silicon wafers were simultaneously placed inside the chamber as reference substrates for the evaluation of coating thickness and morphological characterization of the cross-section. The peak power density (PDD) was obtained from the formula PPD = (Ipeak × Vpeak)/A_{target}, where Ipeak is the current peak, Vpeak is the voltage peak and A_{target} is the entire surface of the sputter target (19.6 cm^2).

The structural characteristics of the DLC coatings were analyzed by Raman spectroscopy using a Thermo Fisher Scientific DXR confocal Raman microscope (Thermo Fisher Scientific, Waltham, MA, USA) with a 532 nm excitation laser. Surface and cross-sectional morphology were examined using a JEOL JSM-7600F field emission scanning electron microscope (SEM) (JEOL, Tokyo, Japan) equipped with an energy-dispersive X-ray spectroscopy (EDS) detector (Bruker XFlash 630, Bruker Nano GmbH, Berlin, Germany). EDS analyses were used to provide semi-quantitative compositional support for the surface observations. EDS measurements were performed using an acceleration voltage of 15 kV and a working distance of approximately 15 mm. Spectra were acquired from multiple representative regions distributed across the analyzed surfaces in order to improve qualitative reproducibility of the compositional observations. Acquisition times were maintained

constant during all measurements to ensure comparable signal conditions between samples. The EDS analyses presented in this research were primarily used as semi-quantitative compositional support for the observed surface degradation morphology and localized corrosion-related features. Therefore, the reported elemental distributions should not be interpreted as statistically representative overall surface compositions. A full statistical compositional analysis based on multiple mapped regions was beyond the scope of the present research and should be addressed in future work involving the quantitative characterization of large area surfaces.

Table 1. Parameters used for the deposition of DLC coatings on AISI 52100 steel using HiPIMS.

Parameters	Etching Ar+	Etching + Cr	CrC	DLC
Voltage (V)	700	700/702	702/690	700
Current (mA)	4	4/284	313/36	36
Power (W)	3	3/200	219/23	25
PPD (W/cm^2)	0	0/500	428/286	178
Pulse amplitude (ms)	50	50/200	200/50	50
Frequency (Hz)	300	300/300	300/300	300
F_{AR} (sccm)	10	10	10	10
Pressure (Torr)	3.61×10^{-3}	3.14×10^{-3}	3.09×10^{-3}	3.53×10^{-3}
Time (s)	1800	1800	2400	2400

Electrochemical characterization was performed using a computer-controlled ACM Instruments (Cartmel, UK) potentiostat in a conventional three-electrode cell configuration. A saturated calomel electrode (SCE) was used as the reference electrode, while a graphite rod served as the counter electrode. The exposed working area of the samples was 1 cm^2.

Synthetic seawater solution was prepared according to controlled laboratory procedures intended to reproduce the ionic aggressiveness of marine chloride-containing environments, following standardized substitute ocean water preparation practices [28], using analytical-grade reagents sequentially dissolved in distilled water under continuous stirring to ensure complete homogenization (Table 2). The initial pH of the electrolyte was adjusted to 8.2 $\pm$ 0.2 with NaOH, representative of marine exposure conditions. The pH was adjusted before testing but was not continuously monitored during exposure.

Table 2. Reagents and quantities used for the preparation of seawater.

Reagent	Quantity (g/L)
Sodium chloride	24.53
Sodium sulfate (anhydrous)	4.09
Magnesium chloride hexahydrate	5.20
Calcium chloride (anhydrous)	1.16
Strontium chloride hexahydrate	0.025
Potassium chloride	0.695
Sodium bicarbonate	0.201
Potassium bromide	0.101
Boric acid	0.027
Sodium fluoride	0.003

All electrochemical measurements were performed at room temperature under static conditions. Prior to electrochemical testing, samples were allowed to stabilize at open circuit potential (OCP) for 60 min to achieve electrochemical stability. Potentiodynamic polarization tests were performed according to ASTM G3, varying the potential from -500 mV to +1500 mV with respect to OCP at a sweep rate of 1 mV·s^{-1}.

Linear polarization resistance (LPR) measurements were performed by polarizing the working electrode between $\pm$15 mV with respect to the open circuit potential (OCP)

at a sweep rate of 1 mV·s^{-1} at regular intervals during 24 h immersion. Electrochemical impedance spectroscopy (EIS) measurements were performed using a sinusoidal perturbation amplitude of 20 mV with respect to the OCP over a frequency range of 0.05 Hz to 10 kHz.

Corrosion rates were estimated according to ASTM G102 using electrochemical parameters derived from polarization resistance. The Stern-Geary constant (B) was determined from the experimentally obtained anodic and cathodic polarization slopes according to:

$$\beta = \frac{\beta_a \beta_c}{2.303(\beta_a + \beta_c)}, \quad (1)$$

and the corrosion current density was estimated as:

$$i_{corr} = \frac{\beta}{R_p}, \quad (2)$$

All electrochemical experiments were performed in duplicate (n = 2), which provided acceptable reproducibility for comparative analysis.

3. Results

3.1. Hipims Parameters [29]

The values of PPD obtained with the voltage, frequency and wide pulse are show in Table 1, only in case of the Cr and Ar plasma used to etch and to deposited the adhesion film of Cr was reached a PPD of 500 W/cm^2 considered as a HIPIMS discharge, obtaining a high metal ionization (ref a). In the case of CrC and DLC layers the carbon presence difficult the ionization since the high ionization energy of carbon [30].

Characterization of DLC Coating

Figure 1 shows the cross-sectional morphology of the DLC coating deposited on AISI 52100 steel using high-power pulsed magnetron sputtering (HiPIMS). The coating exhibits a relatively uniform thickness and continuous morphology, indicating stable deposition under the selected process conditions. A chromium-based intermediate layer is observed between the steel substrate and the top carbon layer, which is expected to improve interfacial adhesion and mitigate stress concentrations resulting from mechanical mismatch between the metal substrate and the amorphous carbon film [16–18].

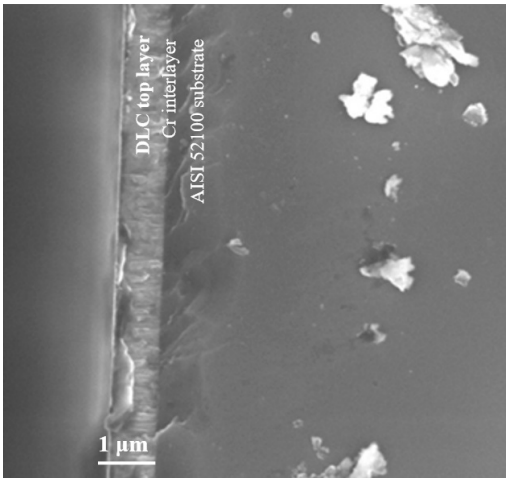


Figure 1. Cross-sectional SEM micrograph of the HiPIMS-deposited DLC coating system showing the DLC top layer, Cr adhesion interlayer, and AISI 52100 steel substrate.

The dense morphology observed in the SEM cross-section image is consistent with the typical microstructural characteristics associated with HiPIMS deposition, where the highly ionized plasma environment promotes energetic ion bombardment, increased adatom mobility, and improved atomic-scale film densification compared to conventional sputtering methods [16–18]. However, the absence of visible large-scale discontinuities in SEM observations should not be interpreted as evidence of a completely defect-free coating architecture, since electrochemical techniques are considerably more sensitive to submicron pathways capable of allowing localized electrolyte entry.

Figure 2 shows the Raman spectra of the analyzed surfaces. The characteristic D (~1350 cm^{-1}) and G (~1580 cm^{-1}) bands observed in the DLC-coated sample confirm the formation of an amorphous carbon structure typical of diamond-like carbon coatings [4–8,31]. The relative intensity and broadening of these bands are consistent with a structurally disordered carbon network containing mixed bonding configurations, as commonly reported for sputter-deposited DLC systems [4–8]. Raman spectral shifts can qualitatively reflect the structural densification and the evolution of internal stresses characteristic of DLC coatings.

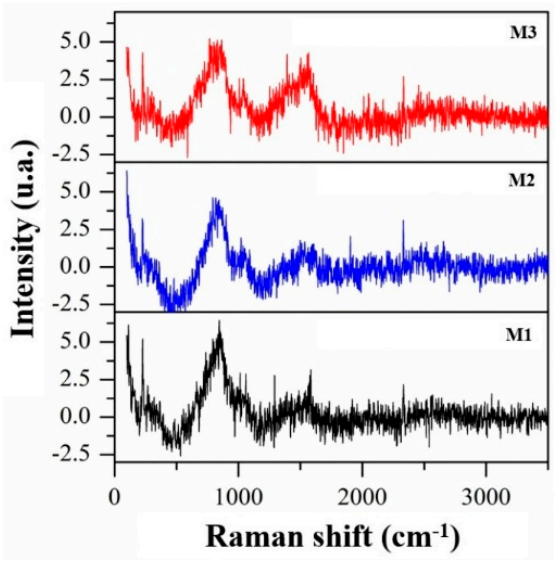


Figure 2. Raman spectra obtained from samples M1 (AISI 52100 steel in its original state), M2 (heat-treated AISI 52100 steel) and M3 (DLC-coated sample using HiPIMS), used for comparative structural characterization of the substrate and coating conditions.

From a corrosion protection perspective, the observed coating continuity and dense morphology suggest an effective restriction of electrolyte transport to the metallic substrate. However, the electrochemical response analyzed in the following sections indicates that access to the electrolyte mediated by localized defects cannot be completely excluded, which is consistent with the expected behavior of practical protective DLC coatings exposed to chloride-containing environments [9–15]. Although the heat treatment applied to AISI 52100 is expected to promote martensitic transformation, the absence of XRD phase quantification prevents direct confirmation of retained austenite fractions. Since retained austenite can influence residual stress distribution, elastic accommodation, and coating adhesion behavior in high-carbon bearing steels, the interpretation of substrate–coating interfacial compatibility should be considered qualitatively. Future work should incorporate XRD phase analysis to establish the relationship between substrate phase constitution and DLC interfacial stability.

Although nanoindentation measurements were not performed in the present investigation due to the limited availability of DLC-coated samples, previous studies on HiPIMS-

deposited DLC coatings under comparable deposition conditions have reported hardness values typically ranging from 18 to 30 GPa, depending on carbon hybridization state, ion bombardment conditions, and interlayer architecture. A comparative literature-based hardness Table 3 was incorporated to provide engineering context regarding the expected mechanical performance of HiPIMS-deposited DLC coatings under similar deposition conditions, as suggested by the reviewer.

Table 3. Comparative hardness values reported for DLC coatings deposited under HiPIMS or related high-ionization sputtering conditions.

Deposition System	Deposition Method	Hardness (GPa)	Ref.
DLC on bearing steel	HiPIMS	18–22	[16]
Cr/DLC multilayer	HiPIMS	20–28	[17]
Hydrogenated DLC	Magnetron sputtering	15–20	[4]
Dense amorphous carbon coating	HiPIMS	22–30	[18]
DLC with Cr interlayer	Pulsed sputtering	18–25	[19]

3.2. Potentiodynamic Polarization Test

Potentiodynamic polarization measurements were performed after stabilization of the open-circuit potential in synthetic seawater. The electrochemical response under the three conditions is presented in Figure 3, while the extracted electrochemical parameters are summarized in Table 4.

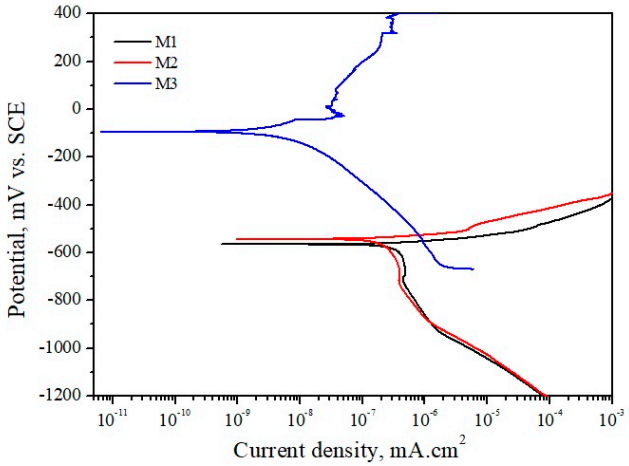


Figure 3. Potentiodynamic polarization curves recorded for the as-received (M1), heat-treated (M2), and HiPIMS DLC-coated (M3) AISI 52100 steel samples in synthetic seawater.

Table 4. Electrochemical parameters obtained from potentiodynamic polarization tests.

Sample	E_{corr} (mV)	I_{corr} (mA/cm^2)	βa (mV/Decade)	βc (mV/Decade)
M1	−564.43	$(1.807 \pm 0.12) \times 10^{-7}$	67	270
M2	−543.02	$(1.000 \pm 0.08) \times 10^{-7}$	80	240
M3	−91.5	$(1.031 \pm 0.09) \times 10^{-9}$	142	116

The substrate in its original state (M1) and the heat-treated steel (M2) exhibited electrochemical behavior characteristic of metallic systems undergoing active corrosion, with relatively high anodic current densities and corrosion potentials located in the active region. These responses indicate limited resistance to chloride-induced electrochemical degradation under the tested conditions, which is consistent with the known susceptibility of AISI 52100 steel in aggressive saline environments [2,3].

In contrast, the DLC-coated condition (M3) showed a marked reduction in the measured current density and a significant shift in the corrosion potential toward more noble

values, indicating a substantially improved electrochemical barrier response compared to uncoated conditions.

However, the polarization response of M3 differs from that of a conventional dissolution-active metal electrode, as expected in a high-strength coated system. Therefore, the electrochemical parameters derived from the polarization adjustment should be interpreted comparatively, rather than as absolute kinetic descriptors of uniform corrosion behavior. In this context, the substantially reduced apparent corrosion current is considered indicative of improved barrier performance and restricted electrolyte access to the metal substrate.

The electrochemical response suggests that the DLC coating deposited by HiPIMS significantly reduces charge transfer processes at the substrate/electrolyte interface. However, this behavior should not be interpreted as evidence of a completely defect-free coating, as localized degradation pathways may still exist due to intrinsic microstructural discontinuities, as discussed in later sections.

3.3. Long-Term Electrochemical Behavior

The long-term electrochemical response of the three experimental conditions was evaluated by monitoring the open-circuit potential (E_{corr}) during 24 h of immersion in synthetic seawater, as shown in Figure 4. The temporal evolution of the corrosion potential provides information on the progressive electrochemical stabilization of the substrate/electrolyte interface and the relative susceptibility of each condition to chloride-induced degradation [15,20–23]. The AISI 52100 (M1) steel in its initial state exhibited the most robust initial corrosion potential, approximately −610 mV against the saturated calomel electrode (SCE), followed by a continuous shift toward more negative values, reaching approximately −732 mV after 24 h of immersion. This sustained negative shift indicates progressive electrochemical activation of the exposed metal surface, consistent with unrestricted access to the electrolyte and ongoing chloride-induced degradation [2,3].

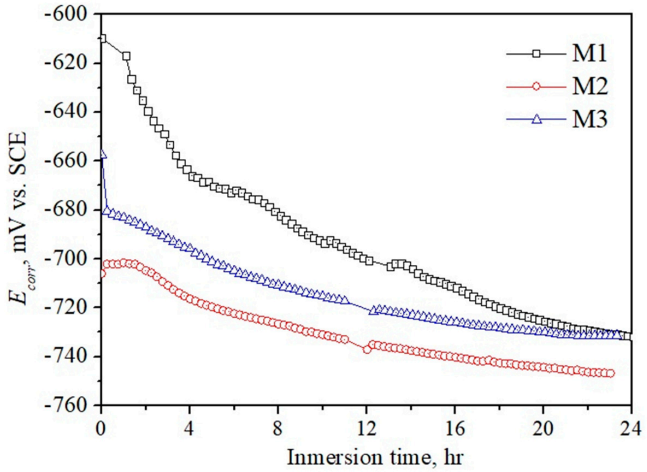


Figure 4. Evolution of the open circuit corrosion potential (Ecorr) of samples M1 (AISI 52100 in original state), M2 (AISI 52100 with heat treatment) and M3 (AISI 52100 coated with DLC by HiPIMS) during 24 h of immersion in synthetic seawater.

This interpretation is supported by the post-exposure surface morphology shown in Figure 5, which exhibits widespread surface deterioration and relatively homogeneous corrosion attack. The absence of a strongly localized deep attack suggests that the degradation process under these conditions was predominantly widespread, consistent with the continuous electrochemical activation of the unprotected substrate during prolonged immersion.

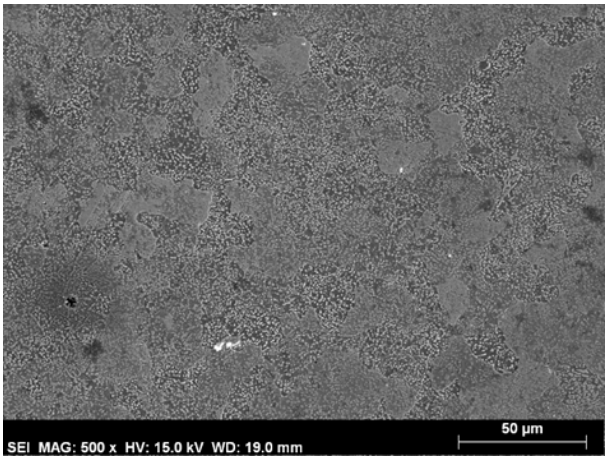


Figure 5. SEM micrograph of the surface of sample M1 after 24 h of immersion in synthetic seawater, showing generalized surface degradation consistent with generalized corrosion of the uncoated AISI 52100 substrate.

The heat-treated condition (M2) exhibited the most negative electrochemical response throughout the immersion period, with an initial potential close to −705 mV against the saturated calomel electrode (SCE) and a gradual evolution to approximately −748 mV after 24 h. This behavior indicates lower electrochemical stability compared to the untreated and DLC-coated conditions, suggesting that the microstructural modifications induced by the heat treatment increased the substrate's susceptibility to chloride-assisted degradation [1–3]. The surface morphology of M2 after exposure, shown in Figure 6, reveals abundant heterogeneous surface deposits distributed across the exposed area, consistent with the accumulation of corrosion products during immersion. The irregular distribution and partial surface coverage suggest the formation of non-uniform degradation products rather than the development of a stable protective surface layer. This observation supports the more active electrochemical response of M2, where persistent access to the electrolyte and continuous interfacial degradation likely contributed to the sustained evolution of the negative potential. The presence of chlorine indicates the active participation of aggressive chloride-containing species in the degradation process. In marine environments, chloride ions are known to destabilize the accumulation of corrosion products, maintain localized electrochemical activity, and accelerate interfacial degradation processes [24,25,27].

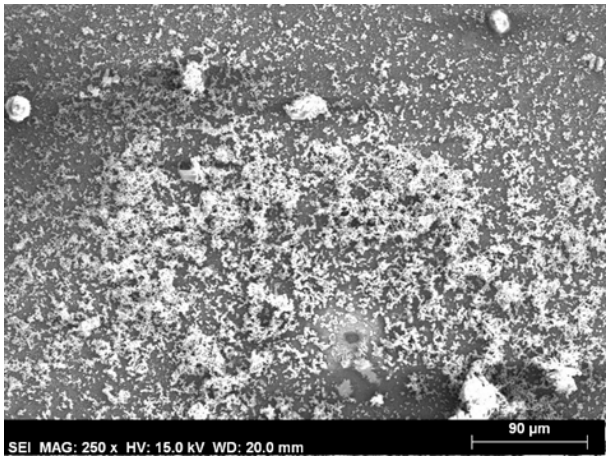


Figure 6. SEM surface micrograph of sample M2 after 24 h immersion in synthetic seawater, showing heterogeneous accumulation of corrosion products associated with active degradation of the heat-treated AISI 52100 substrate.

The DLC-coated condition (M3) exhibited an intermediate electrochemical response, starting near −658 mV against SCE, followed by a relatively rapid initial negative shift and subsequent gradual stabilization to approximately −732 mV after prolonged immersion.

This behavior is characteristic of coated metal systems, where the initial electrochemical response reflects the progressive interaction of the electrolyte with the coating surface and interfacial equilibration processes, rather than the direct, uniform dissolution of the substrate [9–13]. The initial transient may be associated with the wetting and accommodation of the electrolyte in accessible pathways of the coating, while the subsequent, slower evolution suggests a partial restriction of the electrochemical interaction by the coating barrier. The post-exposure morphology of M3, shown in Figure 7, reveals localized surface deposits and scaling of corrosion-related products distributed discontinuously across the coated surface. This morphology suggests that, although the DLC coating substantially restricted electrolyte access compared to uncoated substrates, localized interaction with the corrosive medium still occurred through accessible defect pathways or interfacial discontinuities. The observed detachment could indicate mechanical instability of the accumulated degradation products, rather than the formation of a stable protective corrosion layer.

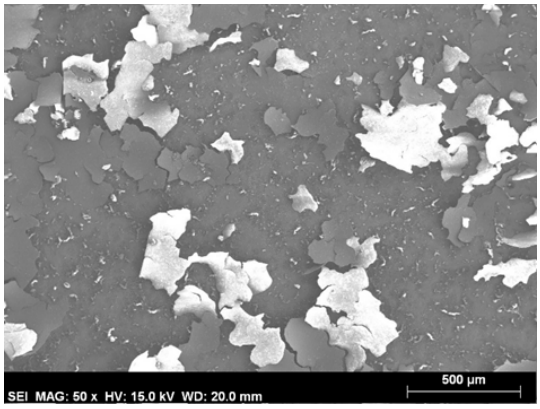


Figure 7. SEM micrograph of the surface of sample M3 after 24 h of immersion in synthetic seawater, showing localized accumulation and partial scaling of corrosion-related surface deposits on the DLC-coated substrate.

The evolution of the apparent corrosion rate, derived from polarization resistance measurements, provides additional information on the temporal electrochemical behavior, as shown in Figure 8. The untreated substrate (M1) exhibited relatively low and stable calculated corrosion rates during immersion, consistent with a relatively constant, generalized electrochemical dissolution process.

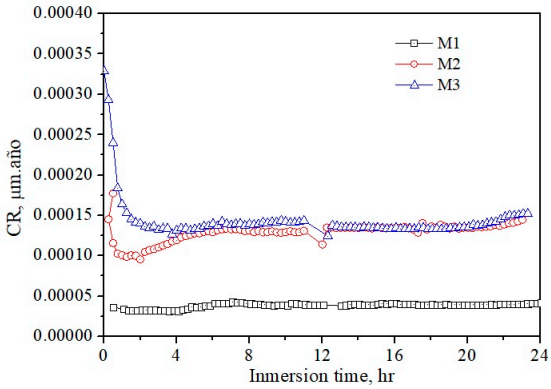


Figure 8. Evolution of the apparent corrosion rate of samples M1, M2 and M3 during 24 h of immersion in synthetic seawater, estimated from polarization resistance measurements.

In contrast, both M2 and M3 showed significantly higher initial apparent corrosion rates, followed by progressive stabilization over time. For the heat-treated substrate (M2), this behavior is consistent with the formation and evolution of unstable and corrosive surface conditions, in accordance with the heterogeneous accumulation of corrosion products observed in Figure 6.

For the DLC-coated condition (M3), the marked initial apparent corrosion rate should be interpreted with caution. In high-strength coated systems, corrosion rate estimates derived from polarization can be strongly influenced by transient interfacial equilibrium, capacitive effects, and model limitations associated with indirect electrochemical fitting [15,20–23], rather than representing direct uniform metal dissolution.

The gradual decrease and subsequent stabilization observed in M3 are therefore more appropriately interpreted as indicative of electrochemical stabilization of the coating/electrolyte interface, rather than direct substrate corrosion kinetics. This interpretation is consistent with the relatively moderate evolution of E_{corr} and the localized surface degradation following exposure shown in Figure 7.

The electrochemical behavior of the DLC coating system deposited by HiPIMS on AISI 52100 steel in synthetic seawater was evaluated using an electrochemically estimated porosity analysis. This provided indirect information on the accessibility of electrolytic pathways mediated by defects at the coating/substrate interface.

Effective electrochemical porosity was estimated using the method proposed by Creus et al. [15], which relates the polarization resistance response of the coated system to that of the uncoated substrate. This methodology does not represent a direct geometric measurement of the coating's physical porosity; rather, it provides an indirect electrochemical indicator of the fraction of the substrate that may be electrochemically accessible through defects or discontinuities in the coating:

$$P = \left(\frac{R_{PS}}{R_P}\right) \times 10^{-(\Delta E_{corr}/\beta_a)}, \quad (3)$$

where R_{PS} represents the polarization resistance of the bare substrate, R_P denotes the polarization resistance of the DLC coating, ΔE_{corr} is the corrosion potential shift, and βa is the anodic Tafel slope of the DLC coating.

The electrochemically estimated effective porosity values decreased from 3.73% after 12 h to 3.06% after 24 h of immersion (Table 5). This trend suggests a progressive reduction in the effective electrochemical accessibility of defect-mediated pathways within the DLC-coated system during prolonged exposure to synthetic seawater.

Table 5. Electrochemical parameters and estimated effective electrochemical porosity of DLC-coated steel after 12 and 24 h immersion in synthetic seawater.

Sample	R_{PS} ($\Omega \cdot cm^2$)	R_P ($\Omega \cdot cm^2$)	$E^{steel}{}_{corr}$ (mV)	E_{corr} (mV)	βa (mV/Decade)	P (%)
DLC_{12}	6359.7	2389.4	−700.62	−721.57	142	3.73
DLC_{24}	6045.3	1953.1	−731.88	−731.33	142	3.06

Since the porosity values were obtained using the electrochemical model proposed by Creus et al. [15], these results should be interpreted as an indirect measure of the fraction of the substrate electrochemically accessible through coating discontinuities, rather than a direct geometric measurement of the coating's physical porosity.

The observed decrease could be associated with progressive interfacial electrochemical stabilization, potentially linked to the localized accumulation of corrosion-related degradation products in accessible coating defects, which could partially restrict ion transport and

increase resistance to charge transfer. However, this interpretation remains indirect, as direct cross-sectional characterization was not performed to confirm the physical obstruction of the defect pathways.

This interpretation is qualitatively supported by the post-exposure surface morphology, shown in Figure 9, where localized features like discontinuities and heterogeneously distributed degradation sites are observed on the DLC-coated surface after 24 h of immersion. These features suggest that, while the coating provided substantial barrier protection, interaction with the electrolyte through localized preferential pathways remained possible. The persistence of effective electrochemical porosity values above 3% further supports the interpretation that a fraction of the substrate remained electrochemically accessible through localized discontinuities in the coating. Under prolonged exposure, this defect-mediated interfacial activity may contribute to progressive coating degradation or localized loss of adhesion.

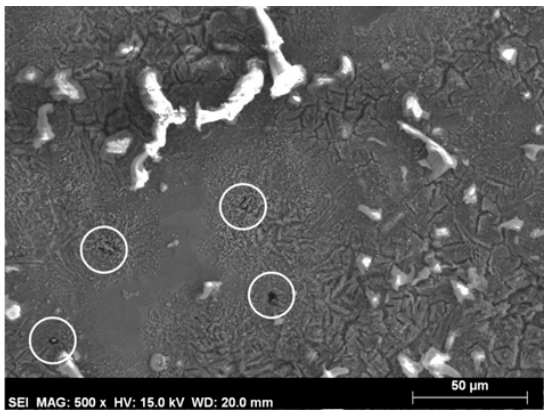


Figure 9. SEM micrograph of the surface of sample M3 after 24 h of immersion in synthetic seawater, showing localized features similar to discontinuities and heterogeneous surface degradation on the DLC-coated substrate.

3.4. Electrochemical Impedance Spectroscopy (EIS) Test

Electrochemical impedance spectroscopy (EIS) measurements performed after 24 h of immersion in synthetic seawater revealed distinct interfacial electrochemical responses for the three evaluated conditions, as shown in Figures 10 and 11. Nyquist and Bode plots demonstrated that the electrochemical behavior of the systems was strongly influenced by the substrate state, the evolution of corrosion products, and the presence of the DLC coating.

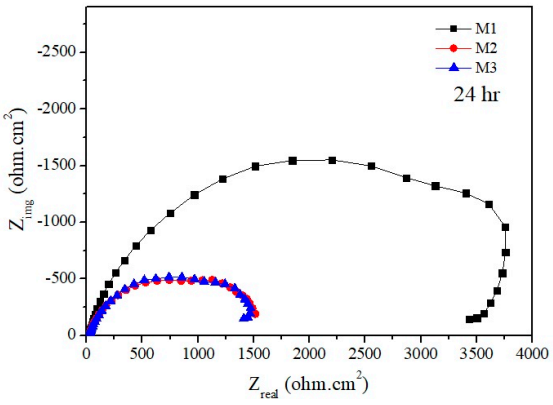


Figure 10. Nyquist plots of samples M1, M2, and M3 after 24 h immersion in synthetic seawater, showing the comparative electrochemical impedance response of the evaluated conditions.

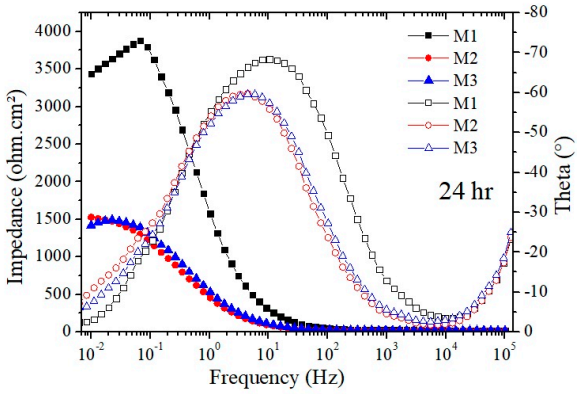


Figure 11. Bode plots of samples M1, M2, and M3 after 24 h immersion in synthetic seawater, illustrating the frequency-dependent electrochemical response of the evaluated systems.

The combined analysis of the impedance response, the equivalent circuit fitting, and the post-exposure SEM/EDS observations (Figures 12–14) provides insights into charge transfer processes, electrolyte accessibility, diffusion-related behavior, and the protective contribution of the DLC coating deposited by HiPIMS under marine chloride exposure conditions [15,20–23].

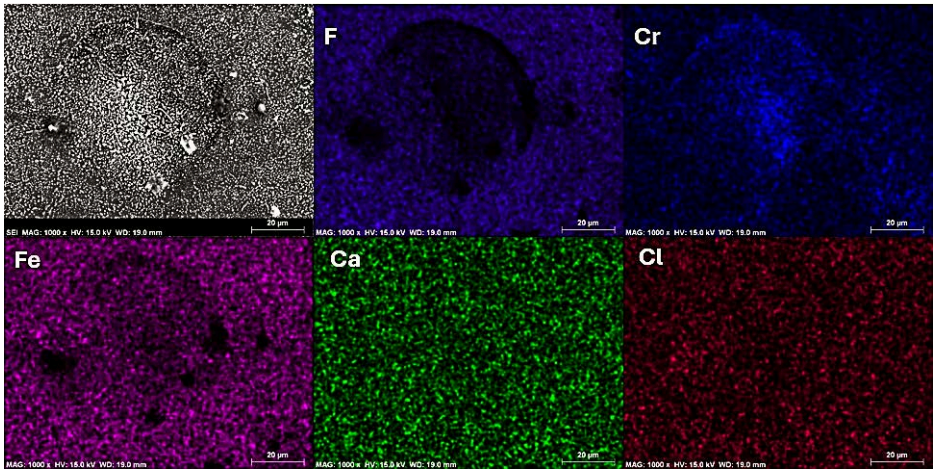
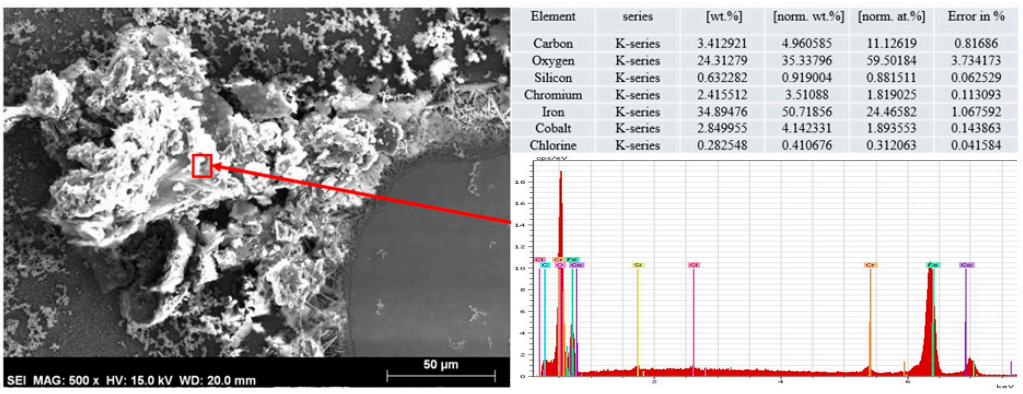


Figure 12. SEM surface micrograph and EDS elemental mapping of the corroded surface after 24 h immersion in synthetic seawater, showing the spatial distribution of Fe, O, Cr, Ca, and Cl on degradation-related surface deposits.



Element	series	[wt.%]	[norm. wt.%]	[norm. at.%]	Error in %
Carbon	K-series	3.412921	4.960585	11.12619	0.81686
Oxygen	K-series	24.31279	35.33796	59.50184	3.734173
Silicon	K-series	0.632282	0.919004	0.881511	0.062529
Chromium	K-series	2.415512	3.51088	1.819025	0.113093
Iron	K-series	34.89476	50.71856	24.46582	1.067592
Cobalt	K-series	2.849955	4.142331	1.893553	0.143863
Chlorine	K-series	0.282548	0.410676	0.312063	0.041584

Figure 13. SEM surface micrograph and localized EDS analysis of corrosion-related deposits formed on sample M2 after 24 h immersion in synthetic seawater.

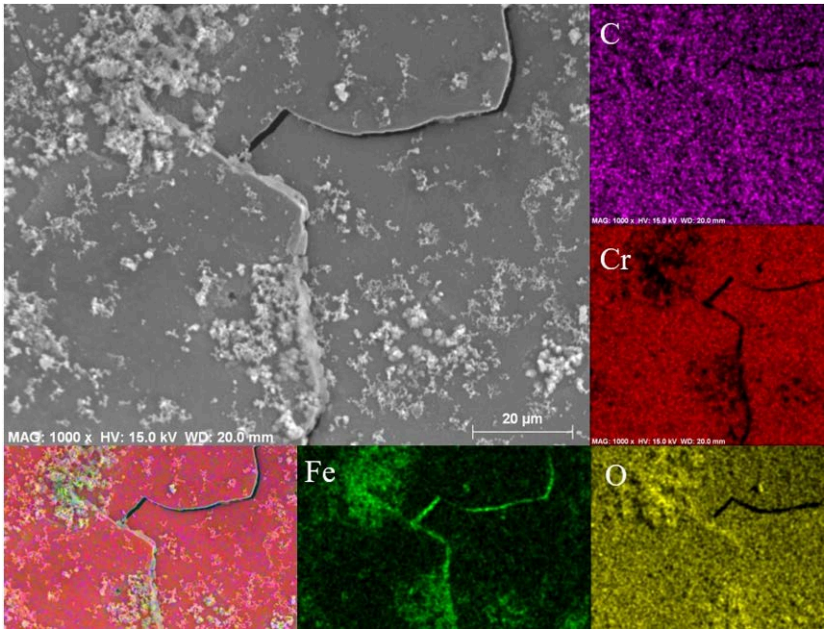


Figure 14. Surface SEM micrography and X-ray elemental mapping of sample M3 after 24 h immersion in synthetic seawater, showing the spatial distribution of C, Cr, Fe and O associated with localized surface heterogeneity related to degradation in the DLC-coated system.

The Nyquist response of sample M1 exhibited the largest capacitive semicircle among the evaluated conditions (Figure 10), indicating the highest apparent impedance response after prolonged immersion. This behavior is consistent with the adjusted charge transfer resistance value obtained from the equivalent circuit analysis (Rct = 2036 $\Omega \cdot cm^2$). However, despite the relatively high impedance magnitude, the electrochemical response of M1 should not be interpreted as evidence of stable passivation of the exposed steel surface. The equivalent electrical circuit used for M1 incorporated a Warburg diffusion contribution, suggesting that the electrochemical behavior was partially controlled by ionic diffusion through corrosion product layers and surface heterogeneities accessible to the electrolyte [15,20–23]. This interpretation is supported by the broad phase angle response observed in the Bode plot (Figure 11), where the non-ideal capacitive behavior indicates electrochemical heterogeneity at the substrate/electrolyte interface.

The surface morphology and elemental distribution shown in Figure 12 provide further evidence of this behavior. SEM/EDS analysis revealed extensive Fe- and O-rich regions associated with the accumulation of corrosion-related degradation products following immersion in synthetic seawater. Localized Cl-containing regions were also detected, indicating the active participation of chloride ions in the degradation process. The widespread distribution of corrosion products on the exposed substrate likely contributed to the increased interfacial resistance by partially restricting ion transport and modifying local electrochemical conditions. However, the progressive negative shift observed in the Ecorr evolution and the presence of the Warburg diffusion element indicate that electrochemical activity and electrolyte accessibility remained active throughout the immersion [24–27].

The heat-treated condition (M2) exhibited a smaller semicircular response on the Nyquist plot and a lower adjusted charge transfer resistance (Rct = 1080 $\Omega \cdot cm^2$), indicating lower interfacial electrochemical stability compared to M1. The Bode response also showed a lower impedance magnitude and greater phase angle dispersion, suggesting a less resistive and more electrochemically active interface. Similar to M1, the equivalent circuit used for M2 incorporated a Warburg diffusion element, indicating that diffusion-assisted electrochemical processes remained relevant in the impedance response. This behavior is consistent with the more negative Ecorr values recorded during immersion and sug-

gests that the microstructural modifications induced by the heat treatment increased the substrate's susceptibility to chloride-assisted electrochemical degradation [1–3].

This interpretation is further supported by the post-exposure morphology presented in Figure 13. SEM observations revealed heterogeneous accumulation of corrosion-related deposits distributed irregularly across the surface, while localized EDS analysis confirmed the presence of Fe, O, C, Cr, Ca, and Cl within the degraded regions. The presence of chlorine-containing species confirms the participation of aggressive chloride ions in the corrosion process, whereas the non-uniform morphology suggests localized electrochemical activity and unstable accumulation of degradation products rather than the formation of a continuous protective layer. Consequently, the lower impedance response observed for M2 can be associated with increased electrolyte accessibility and sustained interfacial electrochemical activity during prolonged immersion.

In contrast, the DLC-coated condition (M3) exhibited a distinct electrochemical response that required a more complex equivalent electrical circuit for satisfactory fitting of the impedance data. The equivalent circuit used for M3 incorporated an additional coating-related time constant composed of a pore resistance element (Rpore = 600 $\Omega \cdot cm^2$) and a coating constant phase element (CPEcoat), indicating that the electrochemical behavior of the system was governed by the combined contribution of the DLC barrier and localized electrolyte penetration through coating discontinuities. The incorporation of Rpore is physically consistent with the electrochemically estimated porosity obtained from the Creus model, where electrolyte accessibility was interpreted as being mediated by localized defect pathways within the coating architecture [15].

The Nyquist response of M3 showed an intermediate semicircular behavior compared to the uncoated conditions, while the Bode diagram revealed a broadened phase-angle response without the ideal capacitive characteristics expected for a completely insulating coating. This behavior indicates that the DLC coating deposited by HiPIMS substantially modified the electrolyte transport processes without fully eliminating electrochemical interaction between the electrolyte and localized substrate regions [9–13]. Unlike M1 and M2, the equivalent circuit of M3 did not require the incorporation of a Warburg diffusion contribution, suggesting that the dominant electrochemical mechanism was no longer governed by diffusion through corrosion-product layers but rather by restricted electrolyte transport through localized coating defects and interfacial discontinuities.

The fitted charge-transfer resistance obtained for M3 (Rct = 1100 $\Omega \cdot cm^2$) was comparable to that of M2, indicating that localized electrochemical activity remained possible at electrochemically accessible regions beneath the coating. However, the presence of the coating-related time constant demonstrates that the DLC layer introduced an additional electrochemical barrier contribution that modified the interfacial response. This interpretation is strongly supported by the elemental mapping presented in Figure 14, where carbon-rich regions associated with the persistence of the DLC coating coexist with localized Fe-, Cr-, and O-containing regions related to interfacial degradation and localized electrolyte accessibility. The observed chemical heterogeneity suggests that the coating remained largely intact after immersion, although localized discontinuities allowed partial penetration of the electrolyte toward the substrate/coating interface. The corresponding equivalent electrical circuits used for fitting are presented in Figure 15, while the tuned electrochemical parameters are summarized in Table 6.

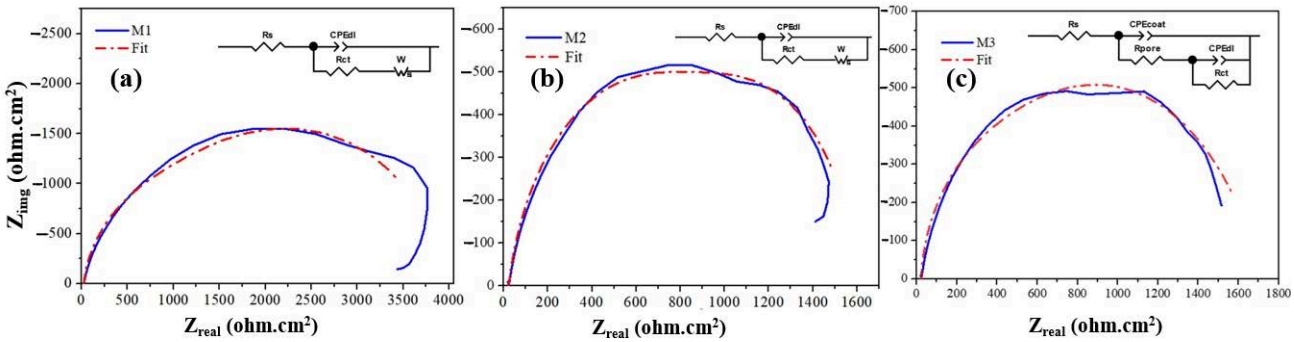


Figure 15. Nyquist plots and equivalent electrical circuit fitting obtained from the EIS response after 24 h immersion in synthetic seawater for: (**a**) M1, (**b**) M2, and (**c**) M3. Symbols correspond to experimental data and dashed lines to fitted responses. The equivalent electrical circuits incorporate the electrochemical contribution of solution resistance (Rs), charge transfer resistance (Rct), constant phase elements (CPE), Warburg diffusion behavior (W), and coating pore resistance (Rpore) associated with defect-mediated electrolyte accessibility in the DLC-coated system.

Table 6. Equivalent circuit fitting parameters obtained from EIS measurements after 24 h immersion in synthetic seawater.

Sample	Rs ($\Omega \cdot cm^2$)	R_{pore} ($\Omega \cdot cm^2$)	$Y_{0,coat}$ (F/cm^2)	n_{coat}	R_{ct} ($\Omega \cdot cm^2$)	Y_{0dl} (F/cm^2)	n_{dl}	*W-R*	*W-T*	*W-P*	x^2
M1	22.87	---	---	---	2036	5.9698×10^{-3}	0.93282	1850	100	0.5	5.6×10^{-4}
M2	22.6	---	---	---	1080	5.9542×10^{-3}	0.86221	500	110	0.5	2.3×10^{-4}
M3	22.27	600	6.62×10^{-5}	0.94871	1100	3.923×10^{-4}	0.6765	---	---	---	2.7×10^{-3}

4. Discussion

The electrochemical behavior of the DLC coating system deposited by HiPIMS on AISI 52100 steel was strongly influenced by the interaction between the coating architecture, the substrate condition, electrolyte accessibility, and defect-mediated interfacial processes. The combined analysis of Raman spectroscopy, polarization measurements, long-term electrochemical evolution, porosity estimation, SEM/EDS observations, and EIS fitting provides evidence that the DLC coating substantially modified the electrochemical response of the substrate in synthetic seawater, although without completely eliminating localized electrolyte accessibility through coating discontinuities.

The Raman spectra presented in Figure 2 confirmed the formation of a characteristic amorphous carbon structure, composed of mixed sp^2/sp^3 bonding configurations, typical of sputter-deposited DLC coatings [4–8]. The broadening and relative intensity of the D and G bands indicate the presence of a structurally disordered carbon network associated with the non-equilibrium growth conditions characteristic of HiPIMS deposition. Previous research has shown that highly ionized deposition environments promote greater adatom mobility and increased film densification, resulting in DLC architectures with improved barrier properties and lower defect density compared to conventional sputtering methods [16–19]. The dense morphology observed in the cross-sectional SEM image (Figure 1) is consistent with this behavior.

From an electrochemical perspective, the Raman response associated with a structurally disordered but relatively dense amorphous carbon network is consistent with the impedance behavior observed during immersion. In particular, the partial restriction of electrolyte accessibility, the presence of coating-related impedance contributions, and the finite Rpore values obtained through equivalent circuit fitting suggest that the HiPIMS process promoted a compact DLC architecture capable of substantially reducing ion transport without completely suppressing defect-mediated electrochemical pathways.

Potentiodynamic polarization results demonstrated a significant reduction in apparent corrosion current density for the DLC-coated condition (M3), decreasing from approximately 10^{-7} to 10^{-9} mA·cm^{-2} compared to uncoated substrates. Simultaneously, the corrosion potential shifted toward more noble values, indicating a substantial modification of the electrochemical interaction between the substrate and the chloride-containing electrolyte. Similar electrochemical improvements have been reported for dense DLC coatings deposited under highly ionized plasma conditions, where the coating acts as a physical barrier restricting electrolyte transport and limiting charge transfer processes at the substrate/electrolyte interface [9–13].

However, the electrochemical response of the coated system should not be interpreted as evidence of complete electrochemical isolation from the substrate. The polarization behavior of M3 differs significantly from that of a conventional metal electrode in active solution, as the measured electrochemical response is governed by the combined contribution of coating capacitance, localized ion transport, and interfacial electrochemical accessibility through coating defects [15,20–23]. Consequently, apparent corrosion current values obtained by polarization fitting should be interpreted comparatively, rather than as absolute descriptors of uniform substrate dissolution kinetics.

The long-term evolution of Ecorr during 24 h of immersion further supports this interpretation. The untreated substrate (M1) showed progressive electrochemical activation characterized by a continuous shift toward more negative potentials, consistent with unrestricted electrolyte accessibility and widespread chloride-induced corrosion. SEM observations after immersion revealed widespread surface degradation and an accumulation of corrosion products distributed relatively homogeneously across the exposed surface. This behavior is characteristic of steel surfaces undergoing active corrosion, where corrosion products partially modify the interfacial electrochemical conditions without establishing stable passivation [24–27].

The heat-treated condition (M2) exhibited the most negative electrochemical response during immersion, indicating lower electrochemical stability compared with both the untreated and coated conditions. This behavior suggests that the microstructural modifications induced by quenching increased the susceptibility of the substrate to chloride-assisted degradation. Although martensitic transformation is expected after the applied heat treatment, the absence of XRD phase quantification prevents direct determination of retained austenite fractions, which may influence residual stress accommodation, coating adhesion, and localized electrochemical response. SEM/EDS observations revealed heterogeneous accumulation of corrosion products containing Fe, O, Cr, Ca, and Cl, indicating unstable interfacial degradation and sustained electrolyte accessibility throughout immersion.

The electrochemically estimated porosity analysis provided additional information regarding the accessibility of defect-mediated pathways within the coated system. According to the Creus model [15], the effective electrochemical porosity decreased from 3.73% after 12 h immersion to 3.06% after 24 h exposure. Since this methodology estimates the fraction of electrochemically accessible substrate rather than the geometric porosity of the coating itself, these values should be interpreted as indirect indicators of localized electrolyte penetration through coating discontinuities.

The progressive reduction in effective electrochemical porosity suggests partial interfacial stabilization during immersion, potentially associated with the localized accumulation of degradation products within accessible coating defects. Such localized obstruction may partially restrict ionic transport and increase resistance to charge transfer during prolonged exposure. However, the persistence of finite porosity values above 3% confirms that a fraction of the substrate remained electrochemically accessible through localized discontinuities in the coating architecture. SEM observations shown in Figure 9 support this

interpretation by revealing heterogeneous degradation sites and localized discontinuities distributed across the coated surface after exposure to synthetic seawater.

The EIS response obtained after 24 h immersion provides the clearest evidence of the electrochemical mechanisms governing the three evaluated systems. The Nyquist and Bode responses demonstrated that the electrochemical behavior was strongly influenced by substrate condition, corrosion-product evolution, and coating-related transport phenomena. For M1 and M2, the equivalent electrical circuits incorporated a Warburg diffusion contribution, indicating that the electrochemical response was partially controlled by diffusion-assisted processes through corrosion-product layers and electrolyte-accessible surface heterogeneities [15,20–23].

The large capacitive semicircle observed for M1 and the comparatively high fitted charge-transfer resistance (Rct = 2036 $\Omega \cdot cm^2$) should therefore not be interpreted as evidence of stable passivation. Instead, the elevated impedance response is more reasonably associated with the transient accumulation of corrosion products and diffusion-controlled interfacial processes occurring on the actively degrading steel surface. This interpretation is fully consistent with the broad phase-angle dispersion observed in the Bode response and with the extensive Fe- and O-rich degradation products identified by SEM/EDS analysis.

Similarly, M2 exhibited lower impedance magnitude and lower fitted charge-transfer resistance (Rct = 1080 $\Omega \cdot cm^2$), indicating increased electrolyte accessibility and sustained electrochemical activity. The incorporation of the Warburg element into the equivalent circuit further supports the interpretation that ionic diffusion through heterogeneous corrosion-product layers remained an important contributor to the electrochemical response. The heterogeneous morphology and chloride-containing degradation products observed by SEM/EDS are fully consistent with this interpretation.

In contrast, the DLC-coated condition (M3) required a more complex equivalent circuit incorporating an additional coating-related time constant composed of a pore resistance element (Rpore) and a coating constant phase element (CPEcoat). The presence of Rpore physically represents the resistance associated with ionic transport through localized coating discontinuities and accessible electrolyte penetration pathways. Consequently, the electrochemical response of the coated system was governed not only by substrate charge transfer processes but also by coating capacitance, localized electrolyte penetration, and restricted ionic transport through defect-mediated pathways.

The fitted Rpore value of 600 $\Omega \cdot cm^2$ confirms that electrolyte penetration through localized coating defects remained possible despite the substantial barrier contribution of the DLC layer. This behavior is consistent with the electrochemically estimated porosity values and with the localized degradation features observed by SEM after immersion. However, the absence of a Warburg diffusion contribution in the M3 equivalent circuit indicates that the dominant electrochemical mechanism differed substantially from that of the uncoated substrates. Instead of diffusion through corrosion-product layers, the electrochemical response of M3 was controlled primarily by coating-modified transport processes and localized interfacial electrochemical accessibility.

The fitted charge-transfer resistance obtained for M3 (Rct = 1100 $\Omega \cdot cm^2$) remained comparable to that of M2, indicating that localized electrochemical activity persisted at electrochemistry.

5. Conclusions

This study evaluated the corrosion behavior of diamond-like carbon (DLC) coatings deposited by HiPIMS on AISI 52100 steel exposed to synthetic seawater, considering the influence of substrate condition, electrochemical response, and post-exposure surface degradation. The following conclusions can be drawn from the results:

1. The electrochemical corrosion behavior of DLC coatings deposited by HiPIMS on AISI 52100 steel exposed to synthetic seawater was strongly influenced by the interaction between the coating architecture, the substrate condition, and defect-mediated electrolyte accessibility. Combined electrochemical and microstructural analyses demonstrated that the DLC coating substantially modified the substrate's electrochemical response by restricting ion transport and reducing the direct interaction of the electrolyte with the steel surface.
2. Raman spectroscopy confirmed the formation of a characteristic amorphous carbon structure, composed of mixed sp^2/sp^3 bond configurations, associated with dense DLC architectures deposited under highly ionized HiPIMS conditions. Cross-sectional SEM observations revealed a continuous coating morphology and the presence of an intermediate chromium layer that contributed to improved interfacial compatibility between the coating and the substrate.
3. Potentiodynamic polarization measurements demonstrated a significant improvement in electrochemical performance for the DLC-coated condition, reducing the apparent corrosion current density from 10^{-7} to 10^{-9} $mA{\cdot}cm^{-2}$ and shifting the corrosion potential toward more noble values compared to uncoated substrates. However, the electrochemical response of the coated system should be interpreted as representative of partial barrier protection, rather than complete electrochemical isolation of the substrate.
4. Long-term Ecorr evolution and surface observations after exposure revealed that both untreated and heat-treated substrates remained highly susceptible to chloride-assisted electrochemical degradation during prolonged immersion. The heat-treated condition exhibited the most negative electrochemical response, suggesting that cooling-induced microstructural modifications increased electrolyte accessibility and interfacial electrochemical activity under marine exposure conditions.
5. Electrochemically estimated porosity analysis indicated that the effective electrochemical accessibility of the coated system decreased from 3.73% after 12 h of immersion to 3.06% after 24 h of exposure. This behavior suggests progressive interfacial electrochemical stabilization associated with a partial restriction of ion transport through localized discontinuities in the coating. However, the persistence of finite porosity values confirms that a fraction of the substrate remained electrochemically accessible through defect-mediated pathways.
6. Electrochemical impedance spectroscopy demonstrated that the electrochemical response of the uncoated substrates was governed by diffusion-assisted interfacial processes, associated with the accumulation of corrosion products and surface heterogeneities accessible to the electrolyte. In contrast, the DLC-coated system required an additional impedance contribution related to the coating, represented by the Rpore and CPEcoat elements, indicating that the electrochemical behavior was controlled by coupled processes involving coating capacitance, localized electrolyte penetration, and restricted charge transfer through coating discontinuities.
7. The absence of a Warburg diffusion contribution in the equivalent circuit of the DLC-coated system suggests that the coating substantially modified the electrolyte transport behavior compared to uncoated conditions. However, the finite Rpore contribution and the persistence of localized degradation features observed by SEM confirm that the protective behavior of the coating was governed by partial electrochemical barrier effects, rather than by a completely defect-free insulating response.
8. Overall, the results demonstrate that DLC coatings deposited using HiPIMS significantly improve the electrochemical stability of AISI 52100 steel in chloride-rich marine environments by reducing electrolyte accessibility and restricting interfacial

electrochemical activity. However, degradation pathways mediated by localized defects remain relevant to the long-term corrosion behavior of the coating system and should be considered when optimizing DLC protective architectures for aggressive service conditions.

Author Contributions: Conceptualization, I.A., E.H. and A.M.; writing—original draft preparation I.A., E.H. and A.M.; formal analysis, I.A., E.H., M.F. and A.M.; writing—review and editing, A.M. and H.C.; methodology E.H. and J.B.; validation, M.F. and A.M.; resources, E.H., M.F., J.B., H.C. and A.M. All authors have read and agreed to the published version of the manuscript.

Funding: This research received no external funding.

Data Availability Statement: The original contributions presented in this study are included in the article. Further inquiries can be directed to the corresponding authors.

Acknowledgments: I.A. wish to express her gratitude to the Secretariat of Science, Humanities, Technology and Innovation (Secihti) for the scholarship received during her postgraduate studies. The authors of this article wish to express their gratitude to the Materials Degradation Laboratory of the FIM-UMSNH for the support provided. During the preparation of this manuscript, the authors used Gemini AI 2.5 Pro as a translation tool from Spanish to English.

Conflicts of Interest: The authors declare no conflicts of interest.

Abbreviations

The following abbreviations are used in this manuscript:

AISI	American Iron and Steel Institute
ASTM	American Society for Testing and Materials
CPE	Constant Phase Element
Cr	Chromium
DLC	Diamond-Like Carbon
EDS	Energy-Dispersive X-ray Spectroscopy
EIS	Electrochemical Impedance Spectroscopy
Ecorr	Corrosion Potential (Open Circuit Corrosion Potential)
Fe	Iron
HiPIMS	High-Power Impulse Magnetron Sputtering
LPR	Linear Polarization Resistance
M1	As-Received AISI 52100 Steel
M2	Heat-Treated AISI 52100 Steel
M3	HiPIMS-Deposited DLC-Coated AISI 52100 Steel
NaOH	Sodium Hydroxide
OCP	Open Circuit Potential
P	Effective Electrochemical Porosity
Rct	Charge Transfer Resistance
Rpore	Coating Pore Resistance
Rs	Solution Resistance
SCE	Saturated Calomel Electrode
SEM	Scanning Electron Microscopy
XRD	X-ray Diffraction

References

1. Li, Y.; Jiang, Z.; Li, L.; Wang, P.; Li, D.; Xue, W.; Duan, D. Wear Behavior and Damage Characterization for AISI 52100 Bearing Steels: Effect of Hardness and Spherical Carbides. *J. Mater. Res. Technol.* **2024**, *30*, 8359–8370. [CrossRef]
2. Wang, W.; Srinivasan, V.; Siva, S.; Albert, B.; Lal, M.; Alfantazi, A. Corrosion Behavior of Deep Cryogenically Treated AISI 420 and AISI 52100 Steel. *Corrosion* **2014**, *70*, 708–720. [CrossRef]

3. Xie, J.; Alpas, A.T.; Northwood, D.O. The Role of Heat Treatment on the Erosion-Corrosion Behavior of AISI 52100 Steel. *Mater. Sci. Eng. A* **2005**, *393*, 42–50. [CrossRef]
4. Robertson, J. Diamond-Like Amorphous Carbon. *Mater. Sci. Eng. R Rep.* **2002**, *37*, 129–281. [CrossRef]
5. Ferrari, A.C.; Robertson, J. Interpretation of Raman Spectra of Disordered and Amorphous Carbon. *Phys. Rev. B* **2000**, *61*, 14095–14107. [CrossRef]
6. Grill, A. Diamond-Like Carbon: State of the Art. *Diam. Relat. Mater.* **1999**, *8*, 428–434. [CrossRef]
7. Lifshitz, Y. Diamond-Like Carbon—Present Status. *Diam. Relat. Mater.* **1999**, *8*, 1659–1676. [CrossRef]
8. Casiraghi, C.; Ferrari, A.C.; Robertson, J. Raman Spectroscopy of Hydrogenated Amorphous Carbons. *Phys. Rev. B* **2005**, *72*, 085401. [CrossRef]
9. Sharma, R.; Barhai, P.K.; Kumari, N. Corrosion Resistant Behaviour of DLC Films. *Thin Solid Film.* **2008**, *516*, 5397–5403. [CrossRef]
10. Fenili, C.P.; de Souza, F.S.; Marin, G.; Probst, S.M.H.; Binder, C.; Klein, A.N. Corrosion Resistance of Low-Carbon Steel Modified by Plasma Nitriding and Diamond-Like Carbon. *Diam. Relat. Mater.* **2017**, *80*, 153–161. [CrossRef]
11. Cao, L.; Liu, J.; Wan, Y.; Pu, J. Corrosion and Tribocorrosion Behavior of W-Doped DLC Coating in Artificial Seawater. *Diam. Relat. Mater.* **2020**, *109*, 108019. [CrossRef]
12. Vicen, M.; Kajánek, D.; Trško, L.; Bokůvka, O.; Buchtík, M.; Florková, Z.; Frkáň, M. Improving of 100Cr6 Steel Corrosion and Wear Properties in Simulated Sea Water Environment by Tungsten-Doped DLC Coating. *Materials* **2023**, *16*, 4334. [CrossRef] [PubMed]
13. Li, S.; Li, H.; Guo, P.; Li, X.; Yang, W.; Ma, G.; Nishimura, K.; Ke, P.; Wang, A. Enhanced Long-Term Corrosion Resistance of 316L Stainless Steel by Multilayer Amorphous Carbon Coatings. *Materials* **2024**, *17*, 2129. [CrossRef] [PubMed]
14. Kolanji, S.; Sivakatatcham, M.; Palani, S. Studies on Nano-Indentation and Corrosion Behavior of Diamond-Like Carbon Coated Stainless Steel (316L). *Trends Sci.* **2024**, *21*, 7677. [CrossRef]
15. Creus, J.; Mazille, H.; Idrissi, H. Porosity Evaluation of Protective Coatings onto Steel, through Electrochemical Techniques. *Surf. Coat. Technol.* **2000**, *130*, 224–232. [CrossRef]
16. García, J.A.; Rivero, P.J.; Barba, E.; Fernández, I.; Santiago, J.A.; Palacio, J.F.; Fuente, G.G.; Rodríguez, R.J. A Comparative Study in the Tribological Behavior of DLC Coatings Deposited by HiPIMS Technology with Positive Pulses. *Metals* **2020**, *10*, 174. [CrossRef]
17. Gómez, I.; Claver, A.; Santiago, J.A.; Fernandez, I.; Palacio, J.F.; Diaz, C.; Mändl, S.; Garcia, J.A. Improved Adhesion of the DLC Coating Using HiPIMS with Positive Pulses and Plasma Immersion Pretreatment. *Coatings* **2021**, *11*, 1070. [CrossRef]
18. Ganesan, R.; Fernandez-Martinez, I.; Akhavan, B.; Matthews, D.T.A.; Sergachev, D.; Stueber, M.; McKenzie, D.R.; Bilek, M.M.M. Pulse Length Selection in Bipolar HiPIMS for High Deposition Rate of Smooth, Hard Amorphous Carbon Films. *Surf. Coat. Technol.* **2023**, *454*, 129199. [CrossRef]
19. Hassan, M.; Qayyum, A.; Ahmad, S.; Mahmood, S.; Shafiq, M.; Zakaullah, M.; Lee, P.; Rawat, R.S. DLC Coating on Stainless Steel by Pulsed Methane Discharge in Repetitive Plasma Focus. *Appl. Surf. Sci.* **2014**, *303*, 187–195. [CrossRef]
20. Stern, M.; Geary, A.L. Electrochemical Polarization: I. A Theoretical Analysis of the Shape of Polarization Curves. *J. Electrochem. Soc.* **1957**, *104*, 56–63. [CrossRef]
21. Mansfeld, F. Use of Electrochemical Impedance Spectroscopy for the Study of Corrosion Protection by Polymer Coatings. *J. Appl. Electrochem.* **1995**, *25*, 187–202. [CrossRef]
22. Orazem, M.E.; Tribollet, B. *Electrochemical Impedance Spectroscopy*, 2nd ed.; John Wiley & Sons: Hoboken, NJ, USA, 2017.
23. Macdonald, J.R. Impedance Spectroscopy. *Ann. Biomed. Eng.* **1992**, *20*, 289–305. [CrossRef]
24. Revie, R.W. *Uhlig's Corrosion Handbook*, 3rd ed.; Wiley: Hoboken, NJ, USA, 2011.
25. Marcus, P. *Corrosion Mechanisms in Theory and Practice*, 3rd ed.; CRC Press: Boca Raton, FL, USA, 2011.
26. Melchers, R.E. Modeling immersion corrosion of structural steels in natural seawater. *Corros. Sci.* **2003**, *45*, 923–940. [CrossRef]
27. Melchers, R.E.; Jeffrey, R. The critical involvement of anaerobic bacterial activity in modelling the corrosion behaviour of mild steel in marine environments. *Electrochim. Acta* **2008**, *54*, 80–85. [CrossRef]
28. Zhang, H.; Cherng, J.-S.; Chen, Q. Recent progress on high power impulse magnetron sputtering (HiPIMS): The challenges and applications in fabricating VO_2 thin film. *AIP Adv.* **2019**, *9*, 035242. [CrossRef]
29. Eliasson, H.; Rudolph, M.; Brenning, N.; Hajihoseini, H.; Zanáška, M.; Adriaans, M.J.; A Raadu, M.; Minea, T.M.; Gudmundsson, J.T.; Lundin, D. Modeling of high power impulse magnetron sputtering discharges with graphite target. *Plasma Sources Sci. Technol.* **2021**, *30*, 115017. [CrossRef]
30. *ASTM D1141-98(2021)*; Standard Practice for the Preparation of Substitute Ocean Water. ASTM International: West Conshohocken, PA, USA, 2021.
31. He, M.; Yeo, C. Evaluation of Thermal Degradation of DLC Film Using a Novel Raman Spectroscopy Technique. *Coatings* **2018**, *8*, 143. [CrossRef]

Disclaimer/Publisher's Note: The statements, opinions and data contained in all publications are solely those of the individual author(s) and contributor(s) and not of MDPI and/or the editor(s). MDPI and/or the editor(s) disclaim responsibility for any injury to people or property resulting from any ideas, methods, instructions or products referred to in the content.